Human Molecular Genetics, 2011, Vol. 20, No. 16 **3161–3175**
doi:10.1093/hmg/ddr218
Advance Access published on May 15, 2011

Long-term and age-dependent restoration of visual function in a mouse model of CNGB3-associated achromatopsia following gene therapy

Livia S. Carvalho[1], Jianhua Xu[2], Rachael A. Pearson[1], Alexander J. Smith[1], James W. Bainbridge[1], Lynsie M. Morris[2], Steven J. Fliesler[3,4,5,6], Xi-Qin Ding[2,*] and Robin R. Ali[1,*]

[1]The Department of Genetics, UCL Institute of Ophthalmology, London, UK, [2]The Department of Cell Biology, University of Oklahoma Health Sciences Center, Oklahoma City, OK, USA, [3]Research Service, Veterans Administration Western New York Healthcare System, [4]Department of Ophthalmology (Ira G. Ross Eye Institute/ Vision Research Center), [5]Department of Biochemistry, University at Buffalo/State University of New York (SUNY) and [6]SUNY Eye Institute, Buffalo, NY, USA

Received March 29, 2011; Revised and Accepted May 11, 2011

Mutations in the *CNGB3* gene account for >50% of all known cases of achromatopsia. Although of early onset, its stationary character and the potential for rapid assessment of restoration of retinal function following therapy renders achromatopsia a very attractive candidate for gene therapy. Here we tested the efficacy of an rAAV2/8 vector containing a human cone arrestin promoter and a human *CNGB3* cDNA in CNGB3 deficient mice. Following subretinal delivery of the vector, CNGB3 was detected in both M- and S-cones and resulted in increased levels of CNGA3, increased cone density and survival, improved cone outer segment structure and normal subcellular compartmentalization of cone opsins. Therapy also resulted in long-term improvement of retinal function, with restoration of cone ERG amplitudes of up to 90% of wild-type and a significant improvement in visual acuity. Remarkably, successful restoration of cone function was observed even when treatment was initiated at 6 months of age; however, restoration of normal visual acuity was only possible in younger animals (e.g. 2–4 weeks old). This study represents achievement of the most substantial restoration of visual function reported to date in an animal model of achromatopsia using a human gene construct, which has the potential to be utilized in clinical trials.

INTRODUCTION

Complete congenital achromatopsia is a devastating hereditary visual disorder, which is associated with a deficient cone-mediated electroretinogram (ERG) response, color blindness, visual acuity loss, pendular nystagmus, extreme light sensitivity and daytime blindness (1–3). Mutations in four different genes have been identified so far as responsible for causing achromatopsia: the cone *alpha* transducin subunit (*GNAT2*), the *alpha*-prime subunit of cone phosphodiesterase (*PDE6C*) and the *alpha* (A) and *beta* (B) subunits of the cone cyclic nucleotide-gated (CNG) channel (*CNGA3* and *CNGB3*, respectively) (3). Among these genes, mutations in *CNGA3* and *CNGB3* account for ~25 and ~50%, respectively, of all achromatopsia cases, while *GNAT2* and *PDE6C* together only affect ~2% of achromatopsia patients (1,3–5). Nystagmus and sensitivity to bright light develop within a few weeks after birth and although these can improve slightly

*To whom correspondence should be addressed at: Department of Genetics, UCL Institute of Ophthalmology, 11-43 Bath Street, London EC1V 9EL, UK. Tel: +44 2076086817; Fax: +442076086991; Email: r.ali@ucl.ac.uk (R.R.A.); Department of Cell Biology, University of Oklahoma Health Sciences Center, 940 Stanton L. Young Blvd., BMSB 553, Oklahoma City, OK 73104, USA. Tel: +1 4052718001 ext. 47966; Fax: +14052713548; Email: xi-qin-ding@ouhsc.edu (X.-Q. D.)

over time, poor visual acuity (20/200 or less) remains stable throughout life (1–3). Hence, achromatopsia is a severe visual impairment and yet a relatively stationary condition. These factors coupled with the potential for rapid assessment of treatment efficacy through evaluation of cone function and visual acuity renders achromatopsia an ideal candidate for gene therapy.

Rod and cone photoreceptor CNG channels are localized to the plasma membrane of the outer segment and play a pivotal role in phototransduction (6,7). Structurally, CNG channels belong to the superfamily of voltage-gated ion channels and comprise two structurally related subunit types, the A and B subunits: CNGA1/B1 in rods and CNGA3/B3 in cones. Heterologous expression studies have shown that the A subunits form the ion-conducting unit, while the B subunits function as modulators (8,9).

Mutations in *CNGA3* and *CNGB3* have been linked to achromatopsia, progressive cone dystrophy and some maculopathies; with mutations in *CNGB3* alone accounting for >50% of all known cases of achromatopsia (5,10–12). Among the mutations in the *CNGB3* gene, the frame-shift mutation Thr383fsX has the highest frequency, accounting for >80% of all *CNGB3* mutant alleles (2,5,13,14). This mutation truncates the pore-forming region and the cytoplasmic C-terminal domain, leading to a null allele. Hence, gene-supplementation therapy would be an appropriate approach to treat the majority of the patients with *CNGB3* mutations.

As for many other types of hereditary retinal disorders, there are currently no effective treatments for cone defects resulting from CNG channel deficiency. Among a variety of novel therapeutic strategies that are under investigation, gene therapy has been shown to be most promising. Indeed, AAV (adeno-associated virus)-mediated gene therapy for inherited retinal disorders has been successful in a variety of animal models, including rodent and canine models of Leber congenital amaurosis (LCA) (15–20), the CNGA3 and GNAT2 deficiency mouse models (21,22) and canine models of CNGB3 mutation/deficiency (23). Gene therapy even has been shown to be capable of generating an additional cone class in dichromate primates (24). Moreover, three independent clinical trials of AAV-mediated gene therapy for LCA caused by RPE65 deficiency have reported clinical benefit (25–27), leading the way for future trials of gene therapy for other forms of inherited retinal dystrophies.

Over the last four years, there has been considerable progress in developing gene therapy for achromatopsia using various animal models. Previous studies have demonstrated restoration of cone function and improvements in photopic vision in a canine model of CNGB3 deficiency and in *Gnat2*$^{-/-}$ and *Cnga3*$^{-/-}$ mouse models following AAV-mediated gene therapy (21–23). Both the *Cnga3*$^{-/-}$ and the *Gnat2*$^{-/-}$ mouse model studies used a mouse cDNA transgene that could in part explain the almost wild-type levels of photopic ERG recovery observed in *Gnat2*$^{-/-}$ mice after treatment (22). The same, however, was not seen in the treated *Cnga3*$^{-/-}$ mice, which only displayed ERG recovery of ~30% of wild-type levels (21). The least improvement in function was observed in the canine *CNGB3*$^{-/-}$ model, where only 10% ERG recovery was seen after treatment (23). This possibly may have been due to the use of the human *CNGB3* transgene; alternatively, the results may be attributed to the relatively modest extent (~30% of total) of retinal area transduced in that study (23). Due to the presence of different cone types in the human retina, the choice of promoter is of crucial importance when considering gene therapy for achromatopsia. In the previously reported *Gnat2*$^{-/-}$ and *CNGB3*$^{-/-}$ gene therapy studies (22,23), PR2.1 (a 2 kb human M/L cone opsin promoter) was used to drive transgene expression. Although PR2.1 is a robust promoter that mediates high levels of expression, it is active only in M/L-cones, not S-cones (28). The *Cnga3*$^{-/-}$ study used a 0.5 kb fragment of the mouse blue opsin promoter that is active in S-cones but is only active in a subset of M-cones (29).

We have previously shown that the phenotype of *Cngb3*$^{-/-}$ mice reflects the symptoms of patients carrying *CNGB3* mutations, namely impaired cone function and early onset, slow progression of cone degeneration (30,31). This similarity makes the *Cngb3*$^{-/-}$ mouse line a valuable model to explore therapeutic interventions for the treatment of CNGB3-associated cone diseases. Taking into account previous gene therapy studies in other models of achromatopsia, our aim was to use this novel model of CNGB3 deficiency to optimize a treatment for the most common form of achromatopsia. We selected a recombinant AAV2/8 vector to deliver a human cDNA transgene driven by a strong human promoter that is active in both S- and M-cones. Congenital achromatopsia has an early onset, but remains mostly stationary in humans, which opens the question as to whether there is a window of time for effective treatment or, due to the stationary aspect of the disease treatment, if outcome is independent of the age at which a patient is treated.

RESULTS

Subretinal injection of an AAV2/8 vector containing a human cone arrestin promoter results in cone-specific transgenic expression in *Cngb3*$^{-/-}$ mice

We constructed a recombinant AAV2/8 viral vector containing a 0.4 kb fragment of the human cone arrestin promoter (hCAR) and the human *CNGB3* cDNA (rAAV2/8_hCAR_h*CNGB3*). The vector was injected subretinally into *Cngb3*$^{-/-}$ mice at post-natal day 15 (P15). Eyes were isolated at 30 days post-injection (PI) and expression of CNGB3 was evaluated by immunohistochemistry. As shown in Figure 1, CNGB3 immunoreactivity was detected in the outer segments in retinal sections prepared from eyes that had received vector, but not in the uninjected controls. Cone-specific *CNGB3* transgene expression was demonstrated in both M- and S-cones by co-labeling with the antibodies against M-opsin and S-opsin, respectively (Fig. 1).

Increased levels of CNGA3 in *Cngb3*$^{-/-}$ mice following *CNGB3* gene delivery

Heterologous expression studies suggest that CNGA3 is the ion-conducting subunit, while CNGB3 functions as a modulator (9,32–34). These studies are supported by the observation that *Cnga3*$^{-/-}$ mice show a complete loss of cone response, while *Cngb3*$^{-/-}$ mice have a residual cone function (30,31,35). We have shown previously that expression of

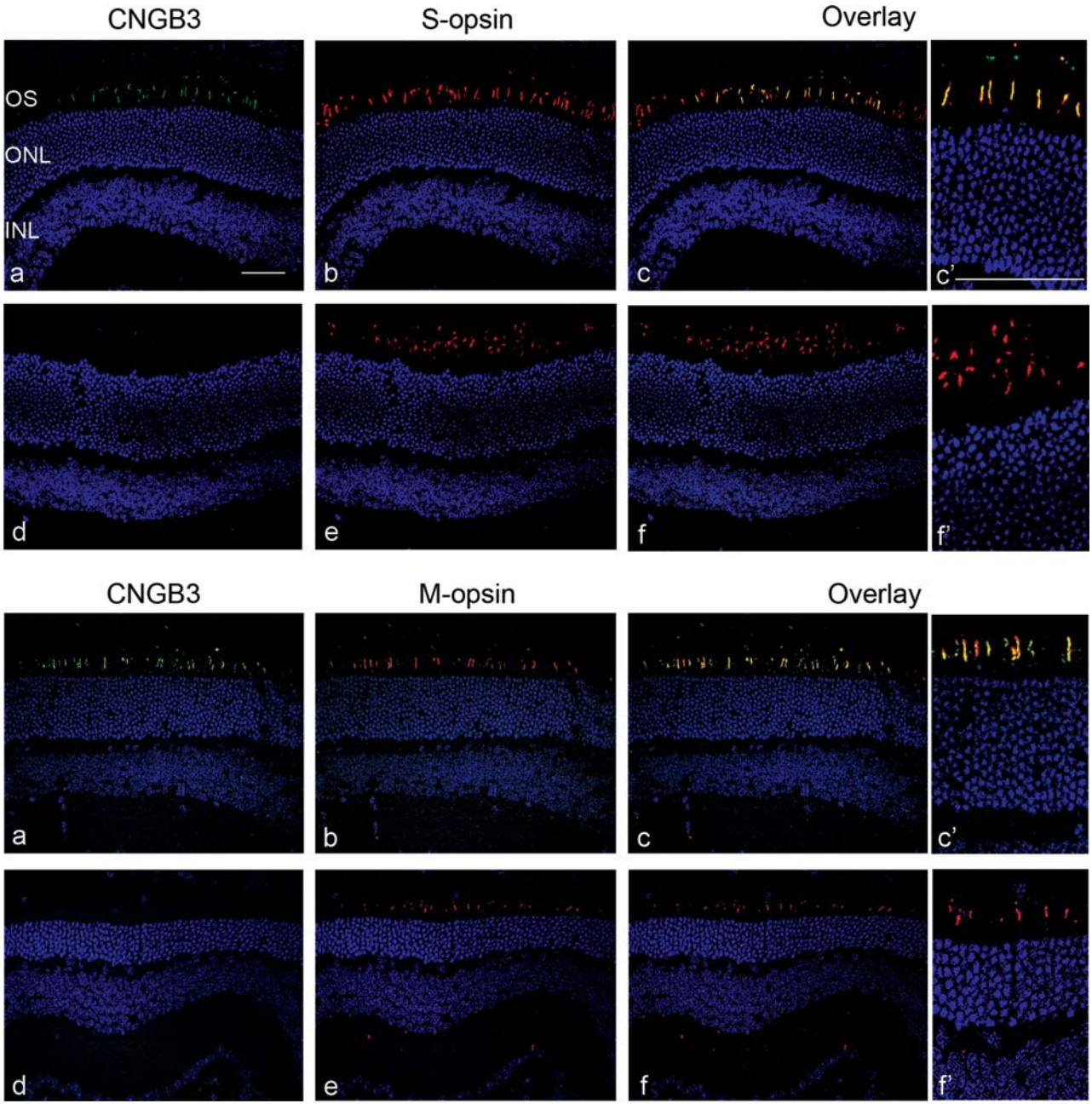

Figure 1. Subretinal injection of AAV2/8 vector containing human cone arrestin promoter results in cone-specific transgenic expression in *Cngb3*$^{-/-}$ mice. Injections were performed at P15 and eyes were collected at 30 days PI to analyze expression of CNGB3. Immunohistochemical detection of CNGB3 expression in the treated (a, b, c) and untreated (d, e, f) *Cngb3*$^{-/-}$ mice. Retinal cross-sections were immunolabeled for CNGB3 (green), S-opsin (red), M-opsin (red) with a nuclear counterstain (DAPI, blue). c′ and f′ are higher magnification images of treated and untreated overlay. Shown are representative images of the analyses from 4 to 6 mice/group. OS, outer segment; ONL, outer nuclear layer; and INL, inner nuclear layer. Scale bars = 50 μm.

Cnga3 is down-regulated in *Cngb3*$^{-/-}$ mice making it likely that the residual cone function in *Cngb3*$^{-/-}$ mice is a function of the remaining CNGA3 homomeric channels and that reduced levels of CNGA3 are responsible for the cone defects in CNGB3 deficiency (31). Therefore, we examined expression of *Cnga3* in the treated eyes to determine whether supplementation of *CNGB3* improves the levels of expression of *Cnga3*. Eye sections, retinal membrane protein preparations and retinal total RNA preparations were used for analyses of *Cnga3* expression. Figure 2A shows improved levels of CNGA3 expression by immunohistochemistry in retinal sections from treated *Cngb3*$^{-/-}$ mice compared with untreated controls and wild-type mice. Figure 2B shows western blot detection of CNGA3 in the treated *Cngb3*$^{-/-}$ mice compared with the untreated controls, wild-type and *Cngb3*$^{+/-}$ mice. Densitometric quantitative analysis (Fig. 2C) shows that the level of CNGA3 in the treated eyes (densitometric units: 25.2 $\pm$ 4.3) was increased significantly ($P < 0.05$) compared with the un-injected controls (densitometric units: 9.6 $\pm$ 2.1), and was comparable to that seen

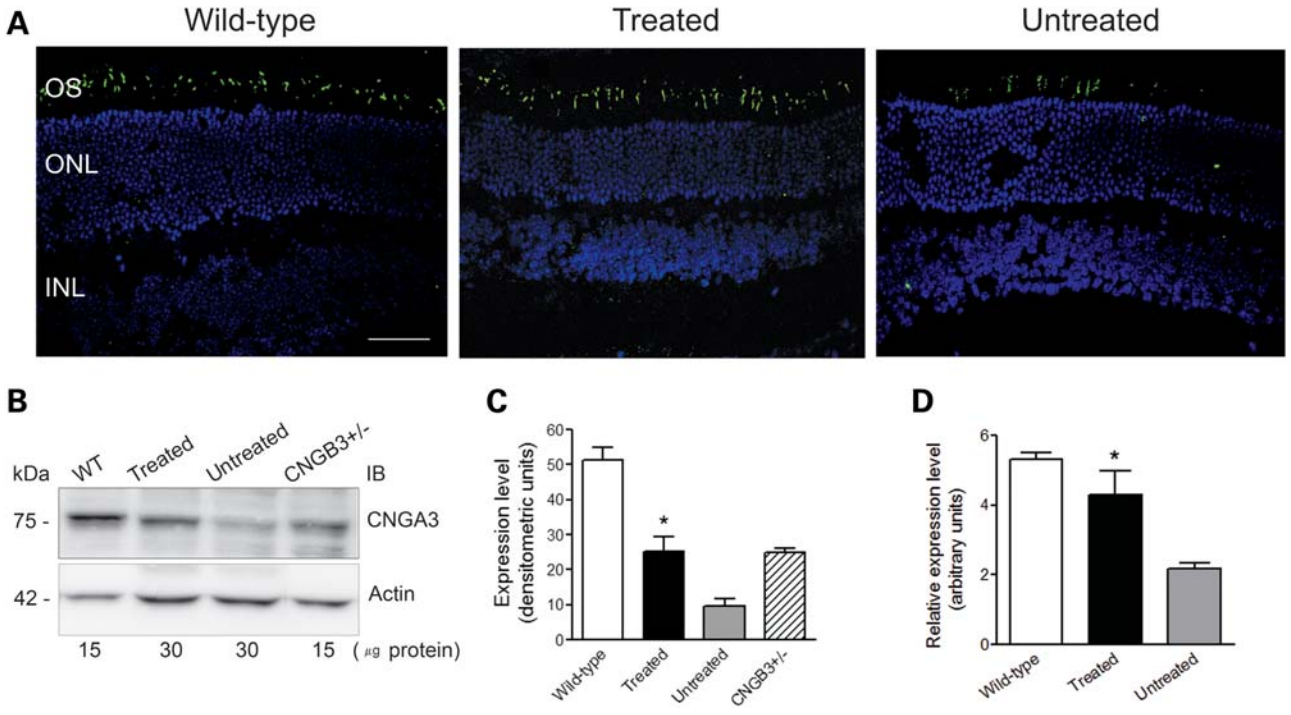

Figure 2. Increased levels of CNGA3 in *Cngb3*$^{-/-}$ mice following h*CNGB3* gene delivery. Viral injections were performed at P15 and eyes were collected at 30 days PI to check for expression of CNGA3. (**A**) Immunohistochemical detection of CNGA3 in the treated and untreated *Cngb3*$^{-/-}$ eyes. Shown are representative images of the analyses from 4 to 6 mice/group. OS, outer segment; ONL, outer nuclear layer; and INL, inner nuclear layer. Scale bars = 50 μm. (**B**) Western blot to detect CNGA3 in eyes from wild-type, *Cngb3*$^{+/-}$ and treated and untreated *Cngb3*$^{-/-}$ mice. Retinal membrane preparations were resolved by 10% SDS–PAGE, followed by immunoblotting using a polyclonal anti-CNGA3 antibody. (**C**) Quantification of western blot analysis in densitometric units. (**D**) qRT–PCR detection of *Cnga3* mRNA expression. Total RNA was prepared and used in the qRT–PCR assays with primers designed for mouse *Cnga3*. Values are means ± SEM ($n = 5–7$ mice/group). Unpaired Student's *t*-test was used for determination of the significance between treated and untreated eyes ($^*P < 0.05$).

in the *Cngb3*$^{+/-}$ mice (densitometric units: 25.0 ± 1.0). Figure 2D shows significant increased expression of *Cnga3* mRNA as analyzed by qRT–PCR ($P < 0.05$). Thus, these results demonstrate that delivery of the *CNGB3* transgene increases the levels of *Cnga3* in *Cngb3*$^{-/-}$ mice by increasing the expression of *Cnga3*.

Improved cone ERG responses in *Cngb3*$^{-/-}$ mice following gene therapy

In order to determine whether gene supplementation leads to long-term restoration of cone function and if there was an optimal age window for effective treatment, vector was injected at P6, 15, 30, 90 and 180. ERG recordings were then performed at monthly intervals, starting at 30 days PI. Figure 3 shows a comparison between representative ERG traces from treated, untreated and wild-type recordings in animals treated at P30 and assessed 120 days PI. We observed substantial rescue of photopic flash and flicker responses in treated animals, while scotopic traces remained unchanged. Averaged ERG recordings measured at 3–4 months PI for all age groups are shown in Figure 4. There was significant improvement in function between treated and untreated eyes in all age groups ($P < 0.05$). However, it is evident from the results that an ideal window for treatment is present around P15–30 and thus the group injected at P30 was selected to evaluate the long-term efficacy of treatment. Figure 5 shows that the photopic ERG response in injected eyes was restored to near wild-type levels in this group and persisted for up to 270 days PI (the longest time point examined here). Moreover, we were able to observe a consistent long-term effect of treatment in all age-treated groups up to 180 days PI (Fig. 6). These experiments show that treatment performed at P15 and P30 achieves a near complete ERG restoration (>90% of wild-type level), while treatment performed at P90 and P180 resulted in functional rescue at 70–80% and 60–70% of wild-type levels, respectively. The group showing the smallest rescue was the group treated at P6, where visual function only reached ∼55% of wild-type levels. This could be explained by the increased amount of retinal damage observed after injection in the P6 animals, most likely caused by the small eye size and increased surgical trauma (data not shown), but the possibility of low vector transduction and, consequently, low *CNGB3* expression levels in these younger treated animals can also not be excluded.

Improved visual acuity in *Cngb3*$^{-/-}$ mice following gene therapy

Untreated *Cngb3*$^{-/-}$ mice have already been shown to have decreased visual acuity as assessed by observing their optomotor responses under photopic conditions (31). As shown earlier, ERG responses demonstrated that functional

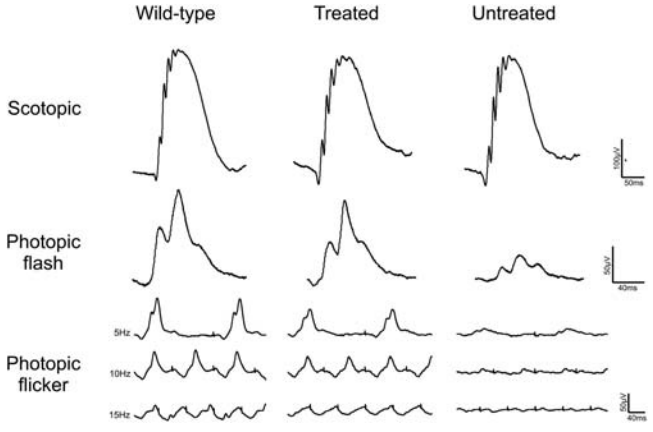

Figure 3. Representative ERG traces from *Cngb3*$^{-/-}$ mice following gene therapy. Wild-type and untreated traces are shown in parallel for comparison. Representative traces shown are from the P30 injected group. Scotopic measurements shown here are from 0.007 cd.s/m^2 intensity. Photopic flash recordings shown are from 10 cd.s/m^2 intensity and flicker recordings are of varying frequencies on a 20 cd.s/m^2 background light.

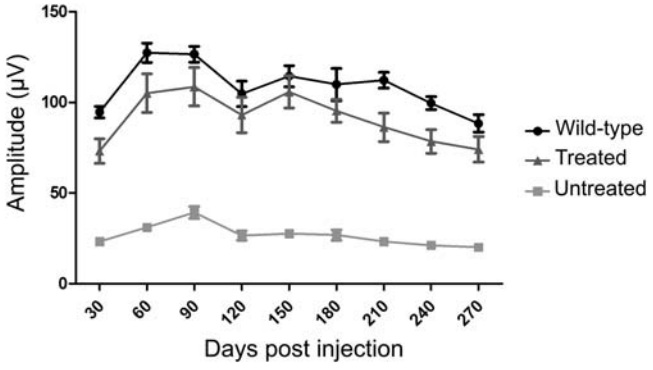

Figure 5. Long-term restoration of cone-mediated ERG following gene therapy. Photopic flash ERGs were recorded at 10 cd.s/m^2. For each time point, data represent the mean ± SEM of measurements from 9–11 eyes for treated and untreated mice; six mice were used for age-matched wild-type controls. Two-way ANOVA was used to determine significance. Treated and untreated groups were statistically significant at all time points ($P < 0.001$), while treated and wild-type groups were not significant at any time point ($P > 0.05$).

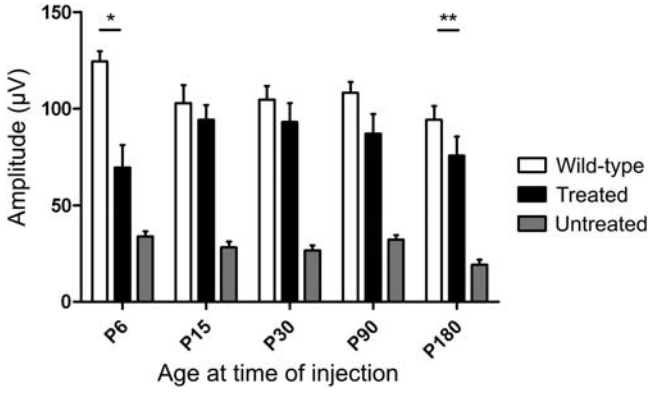

Figure 4. Restoration of cone-mediated ERG in *Cngb3*$^{-/-}$ mice treated at different ages. Data are represented as means ± SEM of photopic b-wave ERG recordings done at 10 cd.s/m^2 measured at *ca* 3–4 months post-injection. Treated and untreated *n* for each group was as follows: P6 = 6; P15 = 6; P30 = 11; P90 = 9; P180 = 6. Wild-type measurements were from 5 to 7 animals. Paired Student's *t*-test was used to determine significance between treated and untreated eyes in all age groups; all showed significance (*P*-values as follows: P6, $P = 0.045$; P15, $P = 0.0017$; P30, $P = 9 \times 10^{-6}$; P90, $P = 0.0006$; P180, $P = 0.0024$. Unpaired Student's *t*-test was used to determine significance between treated and wild-type eyes; only the P6 and P180 groups were significantly different ($^*P = 0.0017$; $^{**}P = 0.0259$).

improvement at the retinal level was possible in both P30 and P180 treated animals, but whether both groups would have the necessary plasticity to restore appropriate behavioral responses was unclear. We therefore examined whether supplementation of the *CNGB3* transgene could improve visual acuity. Two groups of treated *Cngb3*$^{-/-}$ mice (injected at P30 and P180) were tested for their optomotor response (Fig. 7A and B) to examine whether age at treatment had any impact on visual function. As shown in Figure 7C, untreated animals have a significantly lower visual acuity than wild-type (untreated: 0.410 ± SD cycles/degree; $n = 11$; wild-type: 0.525 ± SD cycles/degree; $n = 6$; $P < 0.01$), consistent with a prior report (31). However, after treatment, visual acuity in the P30-treated animals was restored to a similar level (0.520 ± SD cycles/degree; $n = 11$) as that observed in wild-type animals (0.525 ± SD cycles/degree; $n = 6$; $P = 0.83$) In contrast, we observed no significant difference in visual acuity between the treated and untreated eyes in the P180 group (wild-type: 0.510 ± SD cycles/degree; treated: 0.438 ± SD cycles/degree; untreated: 0.410 ± SD cycles/degree; $n = 6$; $P = 0.58$), indicating that treatment received at an older age is less capable of restoring visual acuity. There was no statistical difference in contrast sensitivity between wild-type and treated and untreated *Cngb3*$^{-/-}$ eyes for the either the P30 or P180 groups (Fig. 7C; $P > 0.27$). Therefore, the results presented here show that visual acuity can be restored in *Cngb3*$^{-/-}$ mice by administration of rAAV2/8_hCAR_h*CNGB3*, but there is an inverse correlation between the age of treatment and the degree of improvement in visual function (i.e. the older the age of treatment initiation, the worse the visual function outcome).

Gene therapy improves cone survival in *Cngb3*$^{-/-}$ mice

We have previously shown that cones degenerate in *Cngb3*$^{-/-}$ mice (31). This was evidenced by decreased cone density and decreased expression of cone-specific proteins including cone opsin, cone transducin (GNAT2) and cone arrestin (CAR). In this study, we examined whether administration of rAAV2/8_hCAR_h*CNGB3* improves cone survival. As cone degeneration in *Cngb3*$^{-/-}$ mice occurs early, with decreased cone density already occurring at P30 (30,31), we administered vector at P15 and evaluated cone survival ~8 weeks PI. We found that cone density, as evaluated by peanut agglutinin (PNA) labeling, in the treated eyes (470 ± 17/mm^2) was significantly increased ($P < 0.01$), compared with the untreated eyes (390 ± 12/mm^2 - Fig. 8A, upper panels). In addition, immunofluoresence labeling showed that M-opsin and S-opsin were more abundant in treated (442 ± 7/mm^2 and 472 ± 13/mm^2, respectively) compared

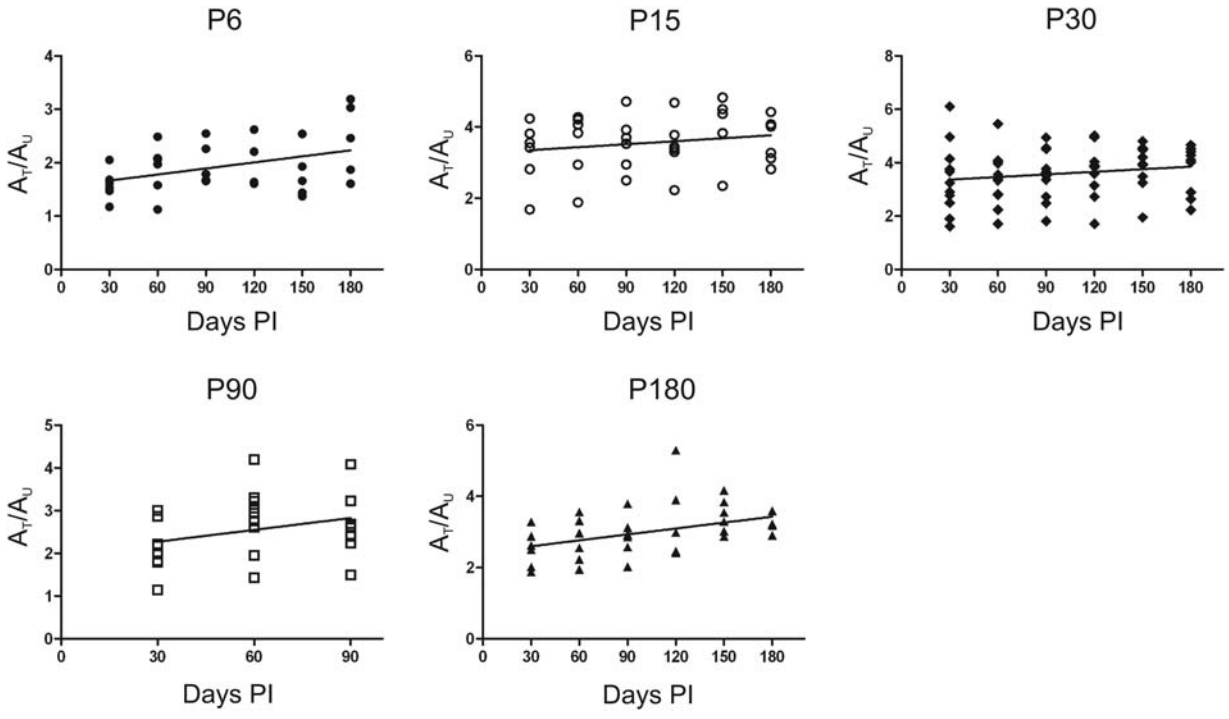

Figure 6. Linear regression analysis of the ratios of b-wave amplitudes from treated/untreated eyes over time. Each panel shows the regression slope for each age group. Each point represents the ratio of b-wave amplitude (10 cd.s/m^2) between treated and untreated eyes (A_T/A_U) for an individual animal at each time point. For all treatment groups the therapeutic effect was maintained over time. The ratio between the photopic ERG response of treated and untreated mice is shown up to 180 days post-injection in all groups, apart from those treated at P90 as these animals were sacrificed at 90 days post-injection to provide samples for the experiments evaluating cone survival and degeneration. *n* numbers varied slightly between groups and time points due to failed ERGs on individual mice on particular days. Although statistical analysis suggests a slight improvement in the P6 and P180 groups, we do not consider these differences biologically relevant ($P = 0.016$ and $P = 0.027$, respectively).

with untreated eyes (367 ± 10/mm^2 and 314 ± 10/mm^2, respectively; Fig. 8A, middle and lower panels). Improved expression of cone-specific proteins, including cone opsin, GNAT2 and CAR was also shown by Western blotting (Fig. 8B).

Reduced cone opsin mis-localization in *Cngb3*$^{-/-}$ mice following treatment

Mis-localization of cone opsins to the inner segments, outer nuclear layer (ONL) and outer plexiform layer (OPL) has been observed in *Cngb3*$^{-/-}$ mice (30). We therefore examined whether expression of the *CNGB3* transgene could improve outer segment localization of cone opsin. As this phenotype was more profound in young mice, we performed injections at P6 and examined localization of cone opsin at P16. Figure 9A shows M-opsin labeling in the treated eyes, compared with untreated eyes. The extent of mis-localization of cone opsin in the ONL and OPL was substantially reduced and cone-opsin labeling was correctly localized to the outer segments in treated eyes and indistinguishable from wild-type controls. Figure 9B shows the quantitative results of the fluorescence intensities of M-opsin labeling in the outer segment, ONL and OPL of the treated mice compared with that in the untreated controls. The fluorescence intensities in ONL and OPL in treated eyes (1.0 ± 0.21 and 3.3 ± 0.74, respectively) were significantly reduced ($P < 0.01$) compared with the untreated eyes (2.9 ± 0.38 and 11.9 ± 1.3, respectively).

Preservation of cone structure in treated *Cngb3*$^{-/-}$ mice

Ultrastructural defects in cone outer segment (COS) structure in *Cngb3*$^{-/-}$ mice has been shown previously (31). While CNGB3 deficiency does not prevent the formation of ultrastructurally normal COSs, it contributes to the subsequent inability of cone cells to maintain normal structural integrity. We examined whether administration of rAAV2/8_hCAR_h*CNGB3* can promote the preservation of normal COS structure in *Cngb3*$^{-/-}$ mice by using transmission electron microscopy (EM). The treatment was performed at P15 and eyes were collected at ~60 days PI and processed for EM analysis. Supplementation with the *CNGB3* transgene effectively preserves COS structure in *Cngb3*$^{-/-}$ mice compared with the untreated *Cngb3*$^{-/-}$ mouse controls. As shown in Figure 10, *Cngb3*$^{-/-}$ cones exhibited ultrastructural abnormalities in their outer segments, including disorganization, misalignment, discontinuities and frank disintegration of disc structure, as well as apparent trapping of cytoplasmic or extracellular matrix material within the space delineated by the COS plasma membrane that formerly housed the intact COS (Fig. 10A and C). In contrast, COS in transgene-treated mice were ultrastructurally normal, well-aligned and intact (Fig. 10B and D). It is important to note that the rod outer

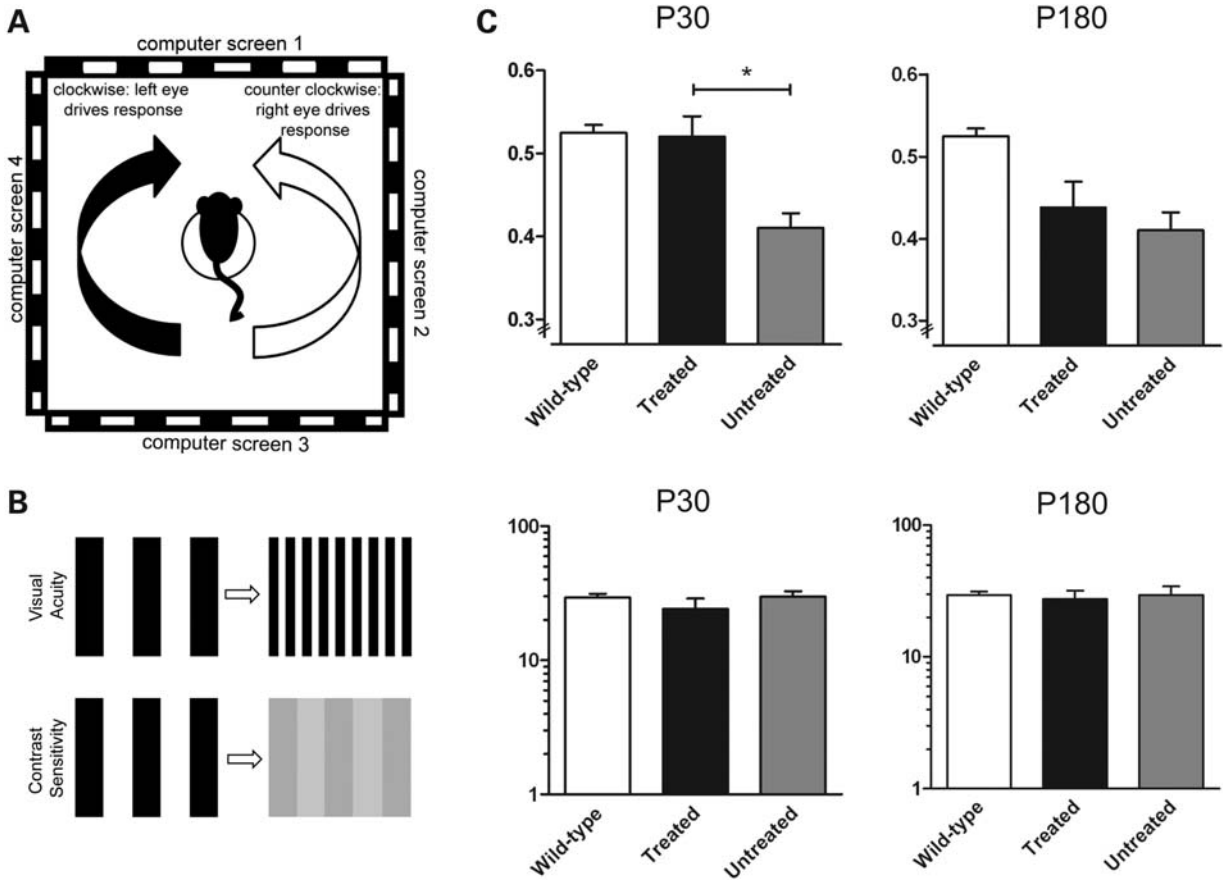

Figure 7. Improved visual acuity in *Cngb3*$^{-/-}$ mice following gene therapy. Visual acuity and contrast sensitivity measurements taken at 60 days post-injection from the *Cngb3*$^{-/-}$ animals treated at P30 and P180. (**A**) Schematic showing the Optomotry© set-up. The mouse sits on a platform surrounded by four computer screens, which project a rotating sinusoidal striped grating. Involuntary reflex head-tracking responses are driven by the left (clockwise rotations, black arrow) and right (counter-clockwise rotations, white arrow) eyes, respectively. (**B**) The set up permits two measures of visual function, contrast sensitivity and visual acuity. (**C**) Visual acuity is restored to wild-type levels in the eyes treated at P30 (top left panel) but not in the eyes treated at P180 (top right panel). Response of the untreated eye remained at ~85–80% of wild-type level. Contrast sensitivity (lower panels) remained the same between treated, untreated and wild-type eyes for both P30 and P180 treated animals. Data are representative as means ± SD of measurements of 11 and 6 eyes for the treated and untreated groups for P30 and P180, respectively, and 12 eyes for wild-type controls. Paired Student's *t*-test was used to determine significance ($P < 0.001$).

segments in both treated and untreated mice were structurally normal; this is expected, since the gene deficiency is cone-specific.

DISCUSSION

Effective gene therapy for achromatopsia requires efficient transgene expression in both S- and M-cones. Here, we describe the first gene therapy for cone-related dystrophies which uses the human CAR promoter to drive transgene expression in cones ubiquitously. Although Michalakis *et al.* (21) were able to show transgene expression (with an S-cone promoter) in both S- and M-cones in the transduced *Cnga3*$^{-/-}$ mouse retina, this could be explained by the high level of S- and M-opsin co-expression in mouse photoreceptors (36). While the S-opsin promoter induced expression in both M- and S-cones in the mouse retina, it may not have the same effect in humans. Therefore, due to the restricted expression in different subsets of cones and possibly bipolar cells (37), neither the PR2.1 nor any blue opsin promoters are as suitable for use in a clinical setting for achromatopsia gene therapy as the CAR promoter which offers specific and robust transgene expression in all types of mouse cones. Komaromy *et al.* (23), however, have previously reported low levels of cone arrestin in the S-cones of dogs and it therefore remains to be seen whether this hCAR is active in all cones in the dog retina and more importantly in all human cone subtypes.

The AAV serotype is another factor that contributes to an efficient transgene delivery. Although the rAAV5 serotype has been shown to transduce a significantly greater number of photoreceptor cells compared with rAAV2 (38), the rAAV8 serotype has an even higher transduction efficiency and has been shown to transduce a higher number of cones than rAAV5 (38–40), potentially making it the ideal choice of vector for achromatopsia gene therapy. Since both the promoter and transgene are of human origin, the construct used in this study would be very suitable for use in patients with achromatopsia.

This study has shown that supplementation of the *CNGB3* transgene also can increase expression of *CNGA3* in

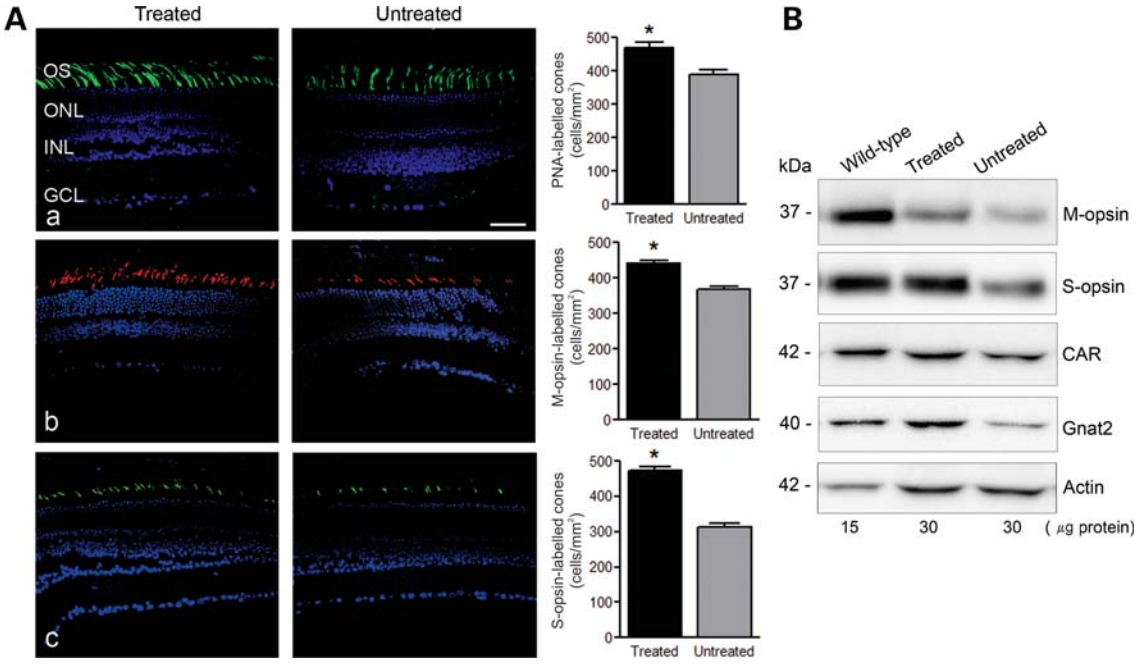

Figure 8. Gene therapy improves cone survival in *Cngb3*$^{-/-}$ mice. Injections were performed at P15 and eyes were collected at 60 days post-injection for PNA lectin cytochemistry and analyses of cone-specific protein expression. (**A**) PNA labeling and cone-opsin staining in the treated *Cngb3*$^{-/-}$ eyes, compared with the untreated control eyes. Retinal sections were analyzed for: (a) PNA lectin staining, (b) M-opsin and (c) S-opsin immunostaining. Shown are representative images of the analysis from 4 to 6 mice/group and correlative quantitative results. OS, outer segment; ONL, outer nuclear layer; INL, inner nuclear layer, GCL, ganglion cell layer. Scale bar: 50 μm. Quantitative results were obtained from 14 to 18 retinal sections prepared from four mice in each group. Unpaired Student's *t*-test was used for determination of the significance ($P < 0.01$). (**B**) Expression of M-opsin, S-opsin, CAR and GNAT2 in the injected-eyes analyzed by western blot analysis. Retinal membrane preparations were resolved by 10% SDS–PAGE, followed by immunoblotting using antibodies against the respective proteins. Shown are representative images of the analysis from 6 to 8 mice/group.

Cngb3$^{-/-}$ mice. CNGA3 is known as the ion-conducting subunit, while CNGB3 is a modulator. In heterologous expression systems, a CNGA3 homomeric channel is fully functional (9,32) and co-expression of CNGB3 with CNGA3 forms heteromeric channels that display a number of properties typical of native CNG channels (9,34). Although CNGB3 shares a common topology with CNGA3 and possesses a pore-forming region, expression of this subunit alone does not form a functional channel (9,32). Taken together, the findings that deficiency of CNGA3 leads to complete loss of cone response (35), while *Cngb3*$^{-/-}$ mice show a residual cone response (31), plus the work showing interaction between CNGA3 and CNGB3 in mouse retina (41), support the cell culture findings. We speculate that the residual cone function in *Cngb3*$^{-/-}$ mice is likely a function of the remaining CNGA3. We have shown a reduced expression of CNGA3 at both the protein and mRNA level in *Cngb3*$^{-/-}$ mice (31); interestingly, a down-regulation of *Cngb3* also was observed in *Cnga3*$^{-/-}$ mice (42). The mechanism by which the two types of the channel subunits inter-regulate each other remains to be identified. Nevertheless, this study showed that supplementation of the *CNGB3* transgene improved expression of the CNGA3 subunit and that the expressed CNGA3 was able to traffic correctly into the outer segments. Thus, the functional rescue in the treated eyes is likely associated with the restoration of the heteromeric channels and an improved expression of CNGA3. Indeed, without sufficient levels of CNGA3, it is unlikely that there would be enough functional channel complexes to sustain cone phototransduction. It is worth noting that the levels of CNGA3 in treated animals did not reach that of wild-type animals (about half the wild-type level, and equivalent to the level of *Cngb3*$^{+/-}$ mice, based on the immunoblotting results). The reason for why the CNGA3 level in treated animals did not reach that of wild-type animals is unknown. It might be related to the expression levels of *CNGB3* transgene or due to a difference between human and mouse CNGB3 subunit. In the wild-type cones there are mouse CNGB3 and CNGA3, while in the treated *Cngb3*$^{-/-}$ cones there are human CNGB3 and mouse CNGA3. The inter-subunit regulation in the two systems might be somewhat different. Nevertheless, this amount of CNGA3 was sufficient for a nearly complete functional rescue. This finding is consistent with the recessive nature of the channelopathies where one *allele* of the gene is sufficient to maintain a normal channel and hence, normal cone function.

The improvement in retinal function in treated *Cngb3*$^{-/-}$ mice was manifested as a long-term recovery of cone ERG responses, with the therapeutic effect maintained for up to 9 months PI. Our best functional rescue was observed in animals treated at P15 and P30. Similar levels of functional rescue reported in this study have only been shown previously in *Gnat2*$^{-/-}$ mice treated at P23–29 with an AAV2/5 vector carrying a mouse *Gnat2* cDNA, where near wild-type level recovery was achieved (22). However, this was achieved by using a mouse, not a human, transgene. The degree of rescue was dependent upon the age at which animals received treatment: treatments performed at P15 and P30 led to a near

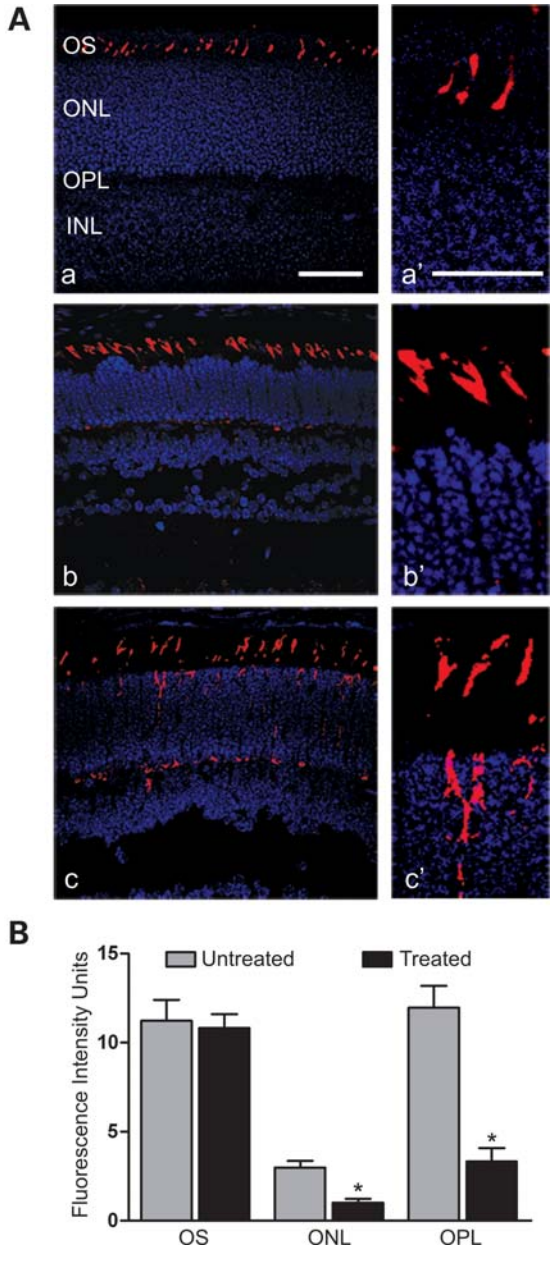

Figure 9. Reduced cone-opsin mis-localization in *Cngb3*$^{-/-}$ mice following gene therapy. The injections were performed at P6 and eyes were collected at P16 for M-opsin labeling. (**A**) Shown are representative images of the analysis from 4 to 6 mice/group for (a) wild-type, (b) treated and (c) untreated eyes, with higher magnification images alongside (a′, b′, c′). OS, outer segment; ONL, outer nuclear layer; and INL, inner nuclear layer. Scale bar: (a) 50 μm, (a′) 25 μm. (**B**) Quantitative analysis of the fluorescence intensities of M-opsin labeling in the OS, ONL and OPL regions. Data represent mean ± SEM and results were obtained from 12 to 14 retinal sections prepared from four mice in each group. Unpaired Student's *t*-test was used for determination of the significance ($P < 0.01$).

complete restoration of photopic ERG responses, while treatment performed at P90 and P180 restored the ERG response to ∼70% of the wild-type level. The reduced effectiveness observed at later ages is likely related to the progression of cone degeneration in older *Cngb3*$^{-/-}$ mice. Our data suggest that treatment at a young age is likely to result in a complete rescue. However, the effectiveness of therapy observed in following treatment of older mice suggests that there is potential for achieving a substantial degree of therapeutic efficacy even for adult patients.

Restored visual acuity in the treated *Cngb3*$^{-/-}$ mice provided further evidence of rescued cone-mediated visual function. The optokinetic reflex permits assessment of visual acuity and contrast sensitivity. Visual acuity is a composite function of cone responses plus inner retinal cell and central visual pathway activities. The successful restoration of visual acuity in the treated *Cngb3*$^{-/-}$ mice suggests that the inner retinal function and the visual pathways involved remain intact in *Cngb3*$^{-/-}$ mice, at least in young animals, and are able to effectively process the input from the recovered cones. It has been shown in mice and squirrel monkeys that visual cortex becomes altered in response to changes in peripheral inputs and that the inner retinal cells and central visual pathways are able to adjust to incorporate an additional cone class (24,43). Studies in achromatopsia patients have also revealed changes in cortical pathways (44). Importantly, we found in this study that in the *Cngb3*$^{-/-}$ mouse model there is some plasticity. Improvement in visual acuity, however, appears to be limited to animals treated at an early age: no improvement in visual acuity was observed in the animals treated at P180. Thus, although good retinal function, as assessed by ERG, can be restored after treatment at all ages and the effectiveness of therapy observed in following treatment of older mice suggests there is potential to treat adult patients, the lack of treatment effect on the visual acuity in the older treated group indicates that an optimal therapeutic window does exist. Without input from photoreceptors for a certain period of time, the inner retina and central visual pathways may permanently lose their ability to reorganize in order to effectively process the input from the recovered cones. Although previous studies had suggested that achromatopsia is a stationary disorder, recent studies using spectral-domain optical coherence tomography measurements of *CNGA3*, *CNGB3* and *PDE6C* patients showed a correlation between age and retinal thickness, suggesting that intervention should occur within the first decade (45–47). Although it is impossible to equate the treatment window found in the mouse model to humans, it is important to keep in mind for future clinical trials that despite the relatively stationary nature of CNGB3-related dystrophies, an optimal window for treatment is likely to exist.

Cngb3$^{-/-}$ mice develop early onset, slow progression of cone degeneration (30). Here, we showed that *CNGB3* transgene supplementation effectively reduced and potentially prevented cone degeneration. The improved cone survival in the treated *Cngb3*$^{-/-}$ eyes was shown by the improvement in cone density, expression of cone proteins and improved structure of COSs. This was seen not only in mice treated at a younger age (P15 days) but also in mice treated at a later age (P90 days). Mice that were injected at P90 days and evaluated at 2 months PI also showed an increased cone density as evaluated by cone opsin labeling and PNA staining (data not shown). Hence, within a certain age range, supplementation of *CNGB3* transgene can ameliorate cone survival. This is in line with the character of slow progression of cone degeneration in CNGB3 deficiency. The mechanism of cone death resulting from CNG channel deficiency is not yet known and

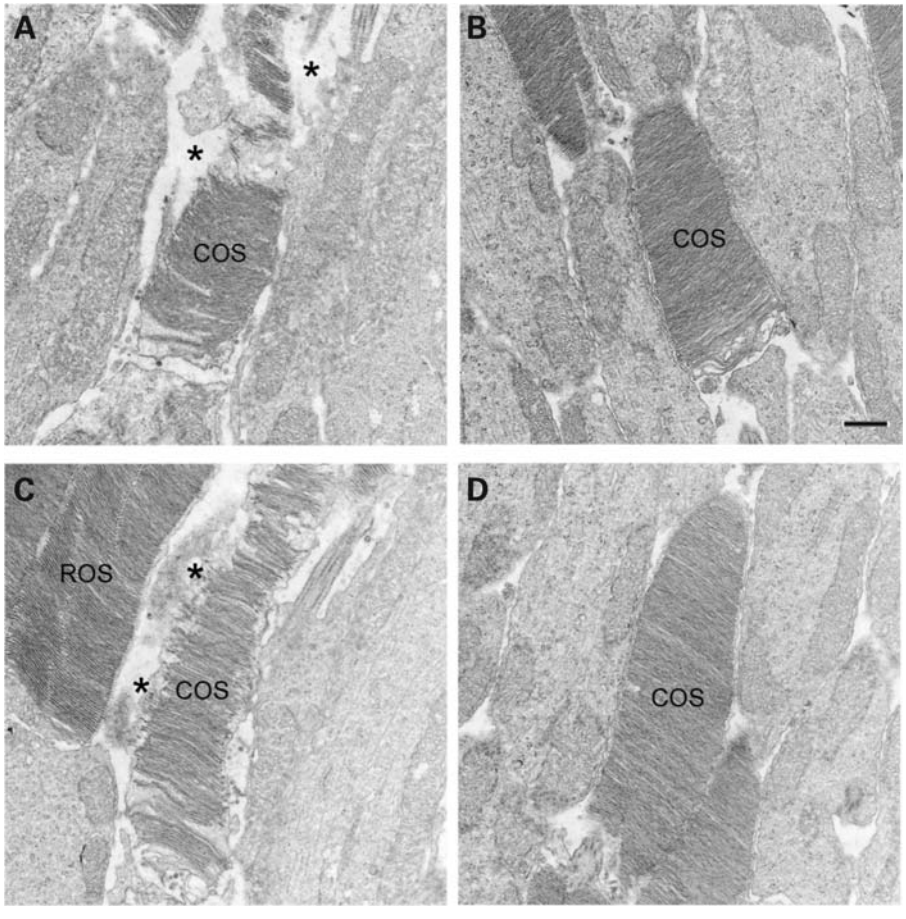

Figure 10. Preservation of cone structure in treated *Cngb3*$^{-/-}$ mice. The treatment was performed at P15 and eyes were collected at 60 days post-injection and processed for transmission EM analysis. Shown are representative images taken from untreated (**A** and **C**) and treated (**B** and **D**) *Cngb3*$^{-/-}$ eyes. COS, cone outer segment; ROS, rod outer segment. Asterisk (*) denotes areas of disintegrated COS, containing undefined matrix material bordered by the COS plasma membrane. Scale bar: 0.5 μm.

may be due to multiple mechanisms. It may be attributed to a decrease or loss of functional channels and subsequent impairment or loss of cone phototransduction altogether. The triggering factors that link phototransduction deficiency with cone death remain to be identified. Cone degeneration in *Cngb3*$^{-/-}$ mice might also be associated with a potential role of CNGB3 in outer segment morphogenesis and maintenance of outer segment integrity, similar to its rod counterpart CNGB1 (the rod CNG channel B subunit), which has been shown to play a role in the morphogenesis of rod outer segment discs (48). Our previous work showing outer segment disorganization in cones of *Cngb3*$^{-/-}$ mice (31) favors this view. In addition, the early onset cone degeneration in *Cngb3*$^{-/-}$ mice might also be related to impaired trafficking/mis-localization of cone opsins, which is profound in developing and young mice; mis-localization of opsin has been correlated with cellular stress and apoptosis (49,50).

In summary, subretinal injection of an rAAV2/8 vector carrying human *CNGB3* driven by a human CAR promoter restored cone function and survival in *Cngb3*$^{-/-}$ mice and improved visual function. As mutations in the *CNGB3* gene are the most prevalent cause for achromatopsia, this study provides proof of concept for a potentially very effective therapy for the major subset of patients with this devastating disorder.

MATERIALS AND METHODS

Animals, antibodies and other materials

Cngb3$^{-/-}$ mouse line (on C57BL/6N background) was generated by targeting deletion (Deltagen Inc., San Mateo, CA) as described previously (31). Wild-type mice (C57BL/6) were purchased from Charles River Laboratories (Wilmington, MA, USA) or Harlan Laboratories (Blackthorn, UK). All mice were maintained under cyclic light (12 h light-dark) conditions; cage illumination was ~7 foot-candles during the light cycle. All experiments were approved by the local Institutional Animal Care and Use Committees (Oklahoma City, USA; UCL, London, UK) and conformed to the guidelines on the care and use of animals adopted by the Society for Neuroscience and the Association for Research in Vision and Ophthalmology (Rockville, MD).

The rabbit polyclonal antibodies against mouse CNGA3 and mouse CNGB3 were generated and characterized as described

previously (31,51). Rabbit polyclonal antibody against mouse S-opsin was provided by Dr Muna Naash (University of Oklahoma Health Sciences Center, Oklahoma City, OK). Affinity purified polyclonal antibodies against mouse M-opsin and cone arrestin were provided by Dr Cheryl Craft (University of Southern California Keck School of Medicine, Los Angeles, CA). Rabbit polyclonal antibody against GNAT2 was obtained from Santa Cruz Biotechnology, Inc. (Santa Cruz, CA). Monoclonal anti-actin antibody was purchased from Abcam, Inc. (Cambridge, MA). Secondary, horseradish peroxidase (HRP)-conjugated anti-rabbit or anti-mouse antibodies were purchased from Kirkegaard & Perry Laboratories Inc. (Gaithersburg, MD). All other chemicals were purchased from Sigma-Aldrich (St Louis, MO), Bio-Rad Laboratories (Hercules, CA) or Invitrogen (Carlsbad, CA).

Construction and production of rAAV2/8.hCAR.hCNGB3

Human *CNGB3* cDNA was a kind gift from Dr Hisao Ueyama (Shiga University of Medial Science, Shiga, Japan) and was cloned into a pD10 vector containing the hCAR (52). The human *CNGB3* gene was inserted in between the hCAR promoter and the SV40 polyadenylation site to generate the construct pD10_hCAR_h*CNGB3*. The construct was then sequenced to verify that no spurious mutations had been incorporated during cloning.

Recombinant AAV2/8 serotype was produced through a previously described tripartite transfection method (53). AAV8 packaging, helper (pHGTI-adeno1) and pD10_h CAR_h*CNGB3* plasmids were transfected into 293T cells with polyethylenimine (PEI; Polysciences, Inc., Eppelheim, Germany) and left for 24 h. The cells were harvested 2 days after transfection and treated with Benzonase (Sigma Aldrich, Dorset, UK) after repeated freeze–thaw cycles to release the vector. Virus preparation was cleared of cellular debris by multiple centrifugation steps followed by previously described purification using ion exchange chromatography (54). The virus preparation was then concentrated in a Vivaspin 4 concentrator (10 kDa, Sartorius Stedim Biotech, Fisher Scientific, Loughborouh, UK) to the desired final volume. Viral genome titer was determined using dot-blot analysis of purified virus preparations and plasmid controls of known concentrations. The AAV2/8_hCAR_h*CNGB3* virus used in this study had a titer of 2×10^{12} viral genomes/ml.

Subretinal injections

All procedures on animals were approved by the local UCL Institute of Ophthalmology Ethics Committee and licensed by the United Kingdom Home Office. Treated animals were divided into five different groups according to the age at injection and subretinal injections of the viral vector were performed on post-natal day (P) 6, P15, P30, P90 and P180 in either the right or left eye (randomly selected) of *Cngb3*$^{-/-}$ mice. The contralateral eye was left as an untreated internal control. Double injections were performed per eye, targeting superior and inferior hemispheres of the retina, as previously described (20). The volume of each injection was determined according to age and eye size of the treated animal as follows: 1.5 μl each for animals injected at P6 and P15 and 2 μl each for animals injected at P30, P90 and P180. Total viral particles delivered per eye were 8×10^9 (P30, P90 and P180) or 6×10^9 (P6 and P15).

Electroretinographic recordings and analysis

ERGs were recorded from both eyes of injected *Cngb3*$^{-/-}$ mice and age-matched wild-type controls on a monthly basis interval starting at 30 days PI with a follow-up of a minimum of 6 months. Un-injected eyes of treated animals were designated as untreated controls. All animals were dark adapted overnight prior to ERG recordings. The animals were prepared for ERG recordings as described previously (20). ERGs were recorded using commercially available equipment (Espion E2, Diagnosys LLC, MA, USA). Bandpass filter cut-off frequencies were 0.312 Hz for the low and 1000 Hz for the hig- frequency cut-off. Scotopic recordings were obtained from dark-adapted animals at the following increasing light intensities: 0.003, 0.007, 0.03 and 0.5 cd.s/m^2. The recordings consisted of 15 responses per intensity with 10 s dark adaptation interval between each. Final response was averaged for each intensity. Photopic recordings were performed following 10 min light adaptation intervals on a background light intensity of 20 cd/m^2, which was also used as the background light for the duration of photopic flash and flicker recordings. Photopic flash recordings consisted of the average of 25 responses for each intensity with a 60 s light adaptation interval between each step. Light intensities used were 0.1, 1, 3, 5, 10 and 20 cd.s/m^2. Photopic flicker recordings consisted of 25 flashes per frequency for 0.5, 2, 5, 10, 15 and 30 Hz. Scotopic b-wave amplitudes were analyzed at a light intensity of 0.007 cd.s/m^2 and photopic at 10 cd.s/m^2.

Statistical analysis

Two-way ANOVA for repeated measures with Bonferroni *post hoc* tests and both paired and unpaired Student's *t*-tests were used to statistically evaluate data. The number of animals for each group was as follows: injected at P6 group, $n = 5$; P15 group, $n = 16$; P30 group, $n = 11$; P90 group, $n = 9$; P180 group, $n = 6$; wild-type group, $n > 5$. Statistical analyses were performed using GraphPad Prism® version 5.01 for Windows (GraphPad Software, San Diego, CA, USA).

Eye preparation, immunohistochemistry and confocal microscopy

Mouse retinal sections were prepared for immunohistochemical analysis as described previously (55,56). Briefly, mouse eyes were enucleated and fixed in 4% formaldehyde in 0.1 M sodium phosphate buffer, pH 7.4, at 4°C overnight. The superior portion of the cornea was marked for orientation prior to enucleation. Fixed eyes were then transferred to PBS or 0.1 M sodium phosphate buffer, pH 7.4, containing 0.02% sodium azide, for storage until processing. Tissue sections were prepared using either a Leica microtome (for paraffin sections, 5 μm thickness) or a Leica cryostat (for frozen sections, 10 μm thickness), respectively.

Table 1. Primers used in this study

Gene symbol	Forward primer	Reverse primers
Hprt	GCAAACTTTGCTTTCCCTGG	CAAGGGCATATCCAACAACA
hCNGB3	AAGTTCTTGGAGGCCCTGAT	GGTTGCTTCTGCGGTCTTAG
mCNGA3	TGCACGACTCTCCCGGAAGTA	ACCGGATAACCCGAGTCTCCA

Immunohistochemical labeling was performed as described previously (31). Briefly, retinal sections were blocked with PBS containing 5% BSA and 0.5% Triton-X 100 for 1 h at room temperature. Primary antibody incubation (anti-CNGB3, 1:200; anti-CNGA3, 1:200; anti-M-opsin, 1:500; and anti-S-opsin, 1:500) was performed at room temperature for 2 h. Following Alexa- or FITC-conjugated secondary antibody incubation and rinses, slides were mounted and cover-slipped. The PNA histochemistry was performed using biotinylated PNA (Vector Laboratories, Burlingame, CA) (1:50) and streptavidin-FITC (Sigma-Aldrich, St Louis, MO). The fluorescent signals were visualized and images were captured using an Olympus AX70 fluorescence microscope (Olympus Corp., Center Valley, PA) with the QCapture® imaging software (QImaging Corp., Surrey, BC, Canada) and an Olympus IX81-FV500 confocal laser scanning microscope (Olympus, Melville, NY) (using excitation wavelengths of 543 nm for Alexa and 488 nm for FITC) with the FluoView® imaging software (Olympus, Melville, NY). Fluorescent labeling intensities of different regions of the retinal sections [outer segment (OS), ONL and OPL] were analyzed using the intensity mapping feature of the software, as described previously (30).

Retinal membrane preparation, SDS–PAGE and western blot analysis

Protein SDS–PAGE and western blotting were performed as described previously (31). Briefly, retinas were homogenized in homogenization buffer (10 mM Tris–HCl, pH 7.4, 1 mM EDTA, 200 mM sucrose, 1 mM phenylmethylsulfonyl fluoride) and the nuclei and cell debris were removed from the homogenate by centrifugation at 1000*g* for 10 min at 4°C. The resulting supernatant was centrifuged at 16 000*g* for 30 min at 4°C, and the resultant membrane pellets were resuspended in buffer and used for western blot analysis.

The retinal membrane proteins were subjected to SDS–PAGE and transferred onto polyvinylidene diflouride membranes. Following 1 h blocking in 5% non-fat milk at room temperature, blots were incubated with primary antibodies at appropriate dilution ratios (anti-M-opsin, 1:2,000; anti-GNAT2, 1:500; anti-CAR, 1:2000; and anti-actin, 1:5000) overnight at 4°C. After 3 × 10 min washings with Tris-buffered saline with 0.1% Tween 20, the blots were incubated with HRP-conjugated secondary antibodies (1:5,000 for anti-actin and 1:25 000 for other antibodies) for 1 h at room temperature. SuperSignal® West Dura Extended Duration chemiluminescent substrate (Pierce, Rockford, IL) was used to detect binding of the primary antibodies to their cognate antigens. Images were captured using a Kodak Imaging Station (4000 R) (Molecular Imaging, New Haven, CT) and densitometry quantification was performed using the Kodak Molecular Imaging software.

RNA isolation and qRT–PCR

Total RNA was isolated from mouse retina using Trizol reagent (Invitrogen, Carlsbad, CA). Two micrograms of total RNA was reverse-transcribed using an oligo-dT primer and SuperScript III reverse transcriptase (Invitrogen, Carlsbad, CA) as per the manufacturer's instructions. Control assays without addition of transcriptase were included and the products were used in the subsequent qRT–PCR as negative controls.

qRT–PCR was performed to detect mRNA levels of mouse *Cnga3*, human *CNGB3* and *HPRT-1*. Primers were designed to generate amplicons of 180–300 bp using Primer3 software (http://frodo.wi.mit.edu/cgi-bin/primer3/primer3_www.cgi). Primers for all genes were designed to span introns to avoid amplification from genomic DNA and are shown in Table 1. The assays were performed on each cDNA sample using a real-time PCR detection system (iCycler; Bio-Rad Laboratories, Hercules, CA). A relative gene expression value △cT was calculated against *HPRT-1* (gene cT − *HPRT-1* cT) for each cDNA sample as described previously (57). Disassociation curve analysis and agarose gel electrophoresis were performed on all PCR products to confirm the proper amplification. The assays were repeated with retinas from at least six animals for each group.

Transmission electron microscopy

Mouse eye samples were prepared for EM as described previously (55,56). Tissue sections were obtained with a Reichert–Jung Ultracut E microtome using a diamond knife. Thin (600–800 Å) sections were collected on copper 75/300 mesh grids for conventional EM analysis and stained with 2% (w/v) uranyl acetate and Reynolds' lead citrate. Sections were viewed with a JEOL 100CX electron microscope at an accelerating voltage of 60 keV and digitized images were collected and stored on a computer for subsequent viewing and analysis.

Evaluation of visual acuity by optomotor testing

Contrast sensitivities and visual acuities of treated and untreated eyes were measured by observing the optomotor responses of mice to rotating sinusoidal gratings (OptoMotry©, Cerebral Mechanics http://www.cerebralmechanics.com/CerebralMechanics_Inc./OptoMotry.html) (58,59). The protocol used yields independent measures of the acuities of right and left eyes based on the unequal sensitivities of the

two eyes to pattern rotation: right and left eyes are most sensitive to counter-clockwise and clockwise rotations, respectively (58,59). A double-blind two-alternative forced choice procedure was employed, in which the observer was 'blind' to the direction of pattern rotation, to whether it was a treated or age-matched wild-type control animal and to which eye received the AAV8/2_hCAR_h*CNGB3* virus injection. Briefly, each mouse was placed on a pedestal located in the centre of four inward facing LCD computer monitors screens and was observed by an overhead infrared video camera with infrared light source (Fig. 7A). Once the mouse became accustomed to the pedestal, a 7s trial was initiated by presenting the mouse with the sinusoidal pattern rotating either clockwise or counter-clockwise as determined randomly by the OptoMotry© software. The observer selected the direction of pattern rotation based on the animal's optomotor response and the monitors returned to 50% gray until the next trial. Acuity was defined as the highest spatial frequency (at 100% contrast) yielding a threshold response, and contrast sensitivity was defined as 100 divided by the lowest percent contrast yielding a threshold response. For photopic acuity, animals were light adapted ($>$60 log cd/m^2) for 30 min prior to testing and the initial stimulus was a 0.200 cycles/degree sinusoidal pattern with a fixed 100% contrast. For photopic contrast sensitivity measurements, the initial pattern was presented at 100% contrast, with a fixed spatial frequency of 0.128 cycles/degree. Visual acuity and contrast sensitivity were measured under photopic conditions (62 log cd/m^2). Visual acuities and contrast sensitivities were measured for both eyes of each mouse at least three times on independent days. Age-matched wild-type mice were tested alongside.

ACKNOWLEDGEMENTS

We thank Drs Hisao Ueyama, Muna Naash and Cheryl Craft for providing the human CNGB3 cDNA, polyclonal anti-S opsin, polyclonal anti-M opsin and polyclonal anti-cone arrestin used in this study. We thank Ms Barbara Nagel for providing excellent technical assistance with electron microscopy.

Conflict of Interest statement. R.R.A. serves on the Clinical Advisory Board of ReGenX LLC.

FUNDING

This work was supported by grants from the National Center for Research Resources (P20RR017703), the NIH (P30EY12190, EY019490 and EY007361), an Unrestricted Grant from Research to Prevent Blindness, the European Union AAVEYE, the British Retinitis Pigmentosa Society and, the Miller Trust. R.R.A. and J.W.B. are supported by the NIHR Biomedical Centre for Ophthalmology at Moorfields Eye Hospital. R.A.P. is a Royal Society University Research Fellow (RG080398). Funding to pay the Open Access publication charges for this article was provided by the Welcome Trust Grant number 082217.

REFERENCES

1. Michaelides, M., Hunt, D.M. and Moore, A.T. (2004) The cone dysfunction syndromes. *Br. J. Ophthalmol.*, **88**, 291–297.
2. Thiadens, A.A., Slingerland, N.W., Roosing, S., van Schooneveld, M.J., van Lith-Verhoeven, J.J., van Moll-Ramirez, N., van den Born, L.I., Hoyng, C.B., Cremers, F.P. and Klaver, C.C. (2009) Genetic etiology and clinical consequences of complete and incomplete achromatopsia. *Ophthalmology*, **116**, 1984–1989.
3. Kohl, S., Jagle, H., Sharpe, L.T. and Wissinger, B. (1993–2004) Achromatopsia. In Pagon, R.A., Bird, T.D., Dolan, C.R. and Stephens, K. (eds), *GeneReviews*. University of Washington, Seattle, USA, Bookshelf ID NBK1418 PMID 20301591 [updated 2010 Dec. 23].
4. Kohl, S., Marx, T., Giddings, I., Jagle, H., Jacobson, S.G., Apfelstedt-Sylla, E., Zrenner, E., Sharpe, L.T. and Wissinger, B. (1998) Total colourblindness is caused by mutations in the gene encoding the alpha-subunit of the cone photoreceptor cGMP-gated cation channel. *Nat. Genet.*, **19**, 257–259.
5. Kohl, S., Varsanyi, B., Antunes, G.A., Baumann, B., Hoyng, C.B., Jagle, H., Rosenberg, T., Kellner, U., Lorenz, B., Salati, R. *et al.* (2005) CNGB3 mutations account for 50% of all cases with autosomal recessive achromatopsia. *Eur. J. Hum. Genet.*, **13**, 302–308.
6. Hirano, A.A., Hack, I., Wassle, H. and Duvoisin, R.M. (2000) Cloning and immunocytochemical localization of a cyclic nucleotide-gated channel alpha-subunit to all cone photoreceptors in the mouse retina. *J. Comp. Neurol.*, **421**, 80–94.
7. Kaupp, U.B., Niidome, T., Tanabe, T., Terada, S., Bonigk, W., Stuhmer, W., Cook, N.J., Kangawa, K., Matsuo, H., Hirose, T. *et al.* (1989) Primary structure and functional expression from complementary DNA of the rod photoreceptor cyclic GMP-gated channel. *Nature*, **342**, 762–766.
8. Zagotta, W.N. and Siegelbaum, S.A. (1996) Structure and function of cyclic nucleotide-gated channels. *Annu. Rev. Neurosci.*, **19**, 235–263.
9. Gerstner, A., Zong, X., Hofmann, F. and Biel, M. (2000) Molecular cloning and functional characterization of a new modulatory cyclic nucleotide-gated channel subunit from mouse retina. *J. Neurosci.*, **20**, 1324–1332.
10. Nishiguchi, K.M., Sandberg, M.A., Gorji, N., Berson, E.L. and Dryja, T.P. (2005) Cone cGMP-gated channel mutations and clinical findings in patients with achromatopsia, macular degeneration, and other hereditary cone diseases. *Hum. Mutat.*, **25**, 248–258.
11. Kohl, S., Baumann, B., Broghammer, M., Jagle, H., Sieving, P., Kellner, U., Spegal, R., Anastasi, M., Zrenner, E., Sharpe, L.T. *et al.* (2000) Mutations in the CNGB3 gene encoding the beta-subunit of the cone photoreceptor cGMP-gated channel are responsible for achromatopsia (ACHM3) linked to chromosome 8q21. *Hum. Mol. Genet.*, **9**, 2107–2116.
12. Wissinger, B., Gamer, D., Jagle, H., Giorda, R., Marx, T., Mayer, S., Tippmann, S., Broghammer, M., Jurklies, B., Rosenberg, T. *et al.* (2001) CNGA3 mutations in hereditary cone photoreceptor disorders. *Am. J. Hum. Genet.*, **69**, 722–737.
13. Johnson, S., Michaelides, M., Aligianis, I.A., Ainsworth, J.R., Mollon, J.D., Maher, E.R., Moore, A.T. and Hunt, D.M. (2004) Achromatopsia caused by novel mutations in both CNGA3 and CNGB3. *J. Med. Genet.*, **41**, e20.
14. Wiszniewski, W., Lewis, R.A. and Lupski, J.R. (2007) Achromatopsia: the CNGB3 p.T383fsX mutation results from a founder effect and is responsible for the visual phenotype in the original report of uniparental disomy 14. *Hum. Genet.*, **121**, 433–439.
15. Acland, G.M., Aguirre, G.D., Ray, J., Zhang, Q., Aleman, T.S., Cideciyan, A.V., Pearce-Kelling, S.E., Anand, V., Zeng, Y., Maguire, A.M. *et al.* (2001) Gene therapy restores vision in a canine model of childhood blindness. *Nat. Genet.*, **28**, 92–95.
16. Pang, J.J., Chang, B., Kumar, A., Nusinowitz, S., Noorwez, S.M., Li, J., Rani, A., Foster, T.C., Chiodo, V.A., Doyle, T. *et al.* (2006) Gene therapy restores vision-dependent behavior as well as retinal structure and function in a mouse model of RPE65 Leber congenital amaurosis. *Mol. Ther.*, **13**, 565–572.
17. Smith, A.J., Schlichtenbrede, F.C., Tschernutter, M., Bainbridge, J.W., Thrasher, A.J. and Ali, R.R. (2003) AAV-Mediated gene transfer slows photoreceptor loss in the RCS rat model of retinitis pigmentosa. *Mol. Ther.*, **8**, 188–195.
18. Pawlyk, B.S., Smith, A.J., Buch, P.K., Adamian, M., Hong, D.H., Sandberg, M.A., Ali, R.R. and Li, T. (2005) Gene replacement therapy rescues photoreceptor degeneration in a murine model of Leber

congenital amaurosis lacking RPGRIP. *Invest. Ophthalmol. Vis. Sci.*, **46**, 3039–3045.
19. Boye, S.E., Boye, S.L., Pang, J., Ryals, R., Everhart, D., Umino, Y., Neeley, A.W., Besharse, J., Barlow, R. and Hauswirth, W.W. (2010) Functional and behavioral restoration of vision by gene therapy in the guanylate cyclase-1 (GC1) knockout mouse. *PLoS One*, **5**, e11306.
20. Tan, M.H., Smith, A.J., Pawlyk, B., Xu, X., Liu, X., Bainbridge, J.B., Basche, M., McIntosh, J., Tran, H.V., Nathwani, A. *et al.* (2009) Gene therapy for retinitis pigmentosa and Leber congenital amaurosis caused by defects in AIPL1: effective rescue of mouse models of partial and complete Aipl1 deficiency using AAV2/2 and AAV2/8 vectors. *Hum. Mol. Genet.*, **18**, 2099–2114.
21. Michalakis, S., Muhlfriedel, R., Tanimoto, N., Krishnamoorthy, V., Koch, S., Fischer, M.D., Becirovic, E., Bai, L., Huber, G., Beck, S.C. *et al.* (2010) Restoration of cone vision in the CNGA3-/- mouse model of congenital complete lack of cone photoreceptor function. *Mol. Ther.*, **18**, 2057–2063.
22. Alexander, J.J., Umino, Y., Everhart, D., Chang, B., Min, S.H., Li, Q., Timmers, A.M., Hawes, N.L., Pang, J.J., Barlow, R.B. *et al.* (2007) Restoration of cone vision in a mouse model of achromatopsia. *Nat. Med.*, **13**, 685–687.
23. Komaromy, A.M., Alexander, J.J., Rowlan, J.S., Garcia, M.M., Chiodo, V.A., Kaya, A., Tanaka, J.C., Acland, G.M., Hauswirth, W.W. and Aguirre, G.D. (2010) Gene therapy rescues cone function in congenital achromatopsia. *Hum. Mol. Genet.*, **19**, 2581–2593.
24. Mancuso, K., Hauswirth, W.W., Li, Q., Connor, T.B., Kuchenbecker, J.A., Mauck, M.C., Neitz, J. and Neitz, M. (2009) Gene therapy for red-green colour blindness in adult primates. *Nature*, **461**, 784–787.
25. Maguire, A.M., Simonelli, F., Pierce, E.A., Pugh, E.N. Jr, Mingozzi, F., Bennicelli, J., Banfi, S., Marshall, K.A., Testa, F., Surace, E.M. *et al.* (2008) Safety and efficacy of gene transfer for Leber's congenital amaurosis. *N. Engl. J. Med.*, **358**, 2240–2248.
26. Bainbridge, J.W., Smith, A.J., Barker, S.S., Robbie, S., Henderson, R., Balaggan, K., Viswanathan, A., Holder, G.E., Stockman, A., Tyler, N. *et al.* (2008) Effect of gene therapy on visual function in Leber's congenital amaurosis. *N. Engl. J. Med.*, **358**, 2231–2239.
27. Cideciyan, A.V., Aleman, T.S., Boye, S.L., Schwartz, S.B., Kaushal, S., Roman, A.J., Pang, J.J., Sumaroka, A., Windsor, E.A., Wilson, J.M. *et al.* (2008) Human gene therapy for RPE65 isomerase deficiency activates the retinoid cycle of vision but with slow rod kinetics. *Proc. Natl Acad. Sci. USA*, **105**, 15112–15117.
28. Wang, Y., Macke, J.P., Merbs, S.L., Zack, D.J., Klaunberg, B., Bennett, J., Gearhart, J. and Nathans, J. (1992) A locus control region adjacent to the human red and green visual pigment genes. *Neuron*, **9**, 429–440.
29. Akimoto, M., Filippova, E., Gage, P.J., Zhu, X., Craft, C.M. and Swaroop, A. (2004) Transgenic mice expressing Cre-recombinase specifically in M- or S-cone photoreceptors. *Invest. Ophthalmol. Vis. Sci.*, **45**, 42–47.
30. Xu, J., Morris, L., Fliesler, S.J., Sherry, D.M. and Ding, X.Q. (2011) early onset, slow progression of cone photoreceptor dysfunction and degeneration in CNG channel subunit CNGB3 deficiency. *Invest. Ophthalmol. Vis. Sci.*, Epub ahead of print January 27, 2011.
31. Ding, X.Q., Harry, C.S., Umino, Y., Matveev, A.V., Fliesler, S.J. and Barlow, R.B. (2009) Impaired cone function and cone degeneration resulting from CNGB3 deficiency: down-regulation of CNGA3 biosynthesis as a potential mechanism. *Hum. Mol. Genet.*, **18**, 4770–4780.
32. Faillace, M.P., Bernabeu, R.O. and Korenbrot, J.I. (2004) Cellular processing of cone photoreceptor cyclic GMP-gated ion channels: a role for the S4 structural motif. *J. Biol. Chem.*, **279**, 22643–22653.
33. Koeppen, K., Reuter, P., Kohl, S., Baumann, B., Ladewig, T. and Wissinger, B. (2008) Functional analysis of human CNGA3 mutations associated with colour blindness suggests impaired surface expression of channel mutants A3(R427C) and A3(R563C). *Eur. J. Neurosci.*, **27**, 2391–2401.
34. Peng, C., Rich, E.D. and Varnum, M.D. (2003) Achromatopsia-associated mutation in the human cone photoreceptor cyclic nucleotide-gated channel CNGB3 subunit alters the ligand sensitivity and pore properties of heteromeric channels. *J. Biol. Chem.*, **278**, 34533–34540.
35. Biel, M., Seeliger, M., Pfeifer, A., Kohler, K., Gerstner, A., Ludwig, A., Jaissle, G., Fauser, S., Zrenner, E. and Hofmann, F. (1999) Selective loss of cone function in mice lacking the cyclic nucleotide-gated channel CNG3. *Proc. Natl Acad. Sci. USA*, **96**, 7553–7557.
36. Applebury, M.L., Antoch, M.P., Baxter, L.C., Chun, L.L., Falk, J.D., Farhangfar, F., Kage, K., Krzystolik, M.G., Lyass, L.A. and Robbins, J.T. (2000) The murine cone photoreceptor: a single cone type expresses both S and M opsins with retinal spatial patterning. *Neuron*, **27**, 513–523.
37. Chiu, M.I. and Nathans, J. (1994) Blue cones and cone bipolar cells share transcriptional specificity as determined by expression of human blue visual pigment-derived transgenes. *J. Neurosci.*, **14**, 3426–3436.
38. Yang, G.S., Schmidt, M., Yan, Z., Lindbloom, J.D., Harding, T.C., Donahue, B.A., Engelhardt, J.F., Kotin, R. and Davidson, B.L. (2002) Virus-mediated transduction of murine retina with adeno-associated virus: effects of viral capsid and genome size. *J. Virol.*, **76**, 7651–7660.
39. Natkunarajah, M., Trittibach, P., McIntosh, J., Duran, Y., Barker, S.E., Smith, A.J., Nathwani, A.C. and Ali, R.R. (2008) Assessment of ocular transduction using single-stranded and self-complementary recombinant adeno-associated virus serotype 2/8. *Gene Ther.*, **15**, 463–467.
40. Allocca, M., Mussolino, C., Garcia-Hoyos, M., Sanges, D., Iodice, C., Petrillo, M., Vandenberghe, L.H., Wilson, J.M., Marigo, V., Surace, E.M. *et al.* (2007) Novel adeno-associated virus serotypes efficiently transduce murine photoreceptors. *J. Virol.*, **81**, 11372–11380.
41. Matveev, A.V., Quiambao, A.B., Browning Fitzgerald, J. and Ding, X.Q. (2008) Native cone photoreceptor cyclic nucleotide-gated channel is a heterotetrameric complex comprising both CNGA3 and CNGB3: a study using the cone-dominant retina of Nrl-/- mice. *J. Neurochem.*, **106**, 2042–2055.
42. Michalakis, S., Geiger, H., Haverkamp, S., Hofmann, F., Gerstner, A. and Biel, M. (2005) Impaired opsin targeting and cone photoreceptor migration in the retina of mice lacking the cyclic nucleotide-gated channel CNGA3. *Invest. Ophthalmol. Vis. Sci.*, **46**, 1516–1524.
43. Jacobs, G.H., Williams, G.A., Cahill, H. and Nathans, J. (2007) Emergence of novel color vision in mice engineered to express a human cone photopigment. *Science*, **315**, 1723–1725.
44. Baseler, H.A., Brewer, A.A., Sharpe, L.T., Morland, A.B., Jagle, H. and Wandell, B.A. (2002) Reorganization of human cortical maps caused by inherited photoreceptor abnormalities. *Nat. Neurosci.*, **5**, 364–370.
45. Thiadens, A.A., Somervuo, V., van den Born, L.I., Roosing, S., van Schooneveld, M.J., Kuijpers, R.W., van Moll-Ramirez, N., Cremers, F.P., Hoyng, C.B. and Klaver, C.C. (2010) Progressive loss of cones in achromatopsia: an imaging study using spectral-domain optical coherence tomography. *Invest. Ophthalmol. Vis. Sci.*, **51**, 5952–5957.
46. Thomas, M.G., Kumar, A., Kohl, S., Proudlock, F.A. and Gottlob, I. (2011) High-resolution in vivo imaging in achromatopsia. *Ophthalmology*, **118**, 882–887.
47. Carroll, J., Choi, S.S. and Williams, D.R. (2008) In vivo imaging of the photoreceptor mosaic of a rod monochromat. *Vision Res.*, **48**, 2564–2568.
48. Zhang, Y., Molday, L.L., Molday, R.S., Sarfare, S.S., Woodruff, M.L., Fain, G.L., Kraft, T.W. and Pittler, S.J. (2009) Knockout of GARPs and the beta-subunit of the rod cGMP-gated channel disrupts disk morphogenesis and rod outer segment structural integrity. *J. Cell Sci.*, **122**, 1192–1200.
49. Chinchore, Y., Mitra, A. and Dolph, P.J. (2009) Accumulation of rhodopsin in late endosomes triggers photoreceptor cell degeneration. *PLoS Genet.*, **5**, e1000377.
50. Tan, E., Wang, Q., Quiambao, A.B., Xu, X., Qtaishat, N.M., Peachey, N.S., Lem, J., Fliesler, S.J., Pepperberg, D.R., Naash, M.I. *et al.* (2001) The relationship between opsin overexpression and photoreceptor degeneration. *Invest. Ophthalmol. Vis. Sci.*, **42**, 589–600.
51. Ding, X.Q., Fitzgerald, J.B., Matveev, A.V., McClellan, M.E. and Elliott, M.H. (2008) Functional activity of photoreceptor cyclic nucleotide-gated channels is dependent on the integrity of cholesterol- and sphingolipid-enriched membrane domains. *Biochemistry*, **47**, 3677–3687.
52. Li, A., Zhu, X. and Craft, C.M. (2002) Retinoic acid upregulates cone arrestin expression in retinoblastoma cells through a Cis element in the distal promoter region. *Invest. Ophthalmol. Vis. Sci.*, **43**, 1375–1383.
53. Gao, G.P., Alvira, M.R., Wang, L., Calcedo, R., Johnston, J. and Wilson, J.M. (2002) Novel adeno-associated viruses from rhesus monkeys as vectors for human gene therapy. *Proc. Natl Acad. Sci. USA*, **99**, 11854–11859.
54. Davidoff, A.M., Ng, C.Y., Sleep, S., Gray, J., Azam, S., Zhao, Y., McIntosh, J.H., Karimipoor, M. and Nathwani, A.C. (2004) Purification of recombinant adeno-associated virus type 8 vectors by ion exchange

chromatography generates clinical grade vector stock. *J. Virol. Methods*, **121**, 209–215.
55. Ding, X.Q., Nour, M., Ritter, L.M., Goldberg, A.F., Fliesler, S.J. and Naash, M.I. (2004) The R172W mutation in peripherin/rds causes a cone-rod dystrophy in transgenic mice. *Hum. Mol. Genet.*, **13**, 2075–2087.
56. Chakraborty, D., Ding, X.Q., Conley, S.M., Fliesler, S.J. and Naash, M.I. (2009) Differential requirements for retinal degeneration slow intermolecular disulfide-linked oligomerization in rods versus cones. *Hum. Mol. Genet.*, **18**, 797–808.
57. Farjo, R., Skaggs, J., Quiambao, A.B., Cooper, M.J. and Naash, M.I. (2006) Efficient non-viral ocular gene transfer with compacted DNA nanoparticles. *PLoS One*, **1**, e38.
58. Umino, Y., Solessio, E. and Barlow, R.B. (2008) Speed, spatial, and temporal tuning of rod and cone vision in mouse. *J. Neurosci.*, **28**, 189–198.
59. Douglas, R.M., Alam, N.M., Silver, B.D., McGill, T.J., Tschetter, W.W. and Prusky, G.T. (2005) Independent visual threshold measurements in the two eyes of freely moving rats and mice using a virtual-reality optokinetic system. *Vis. Neurosci.*, **22**, 677–684.